Supplementary Information: Rules of Contact Inhibition of Locomotion for Cells on Suspended Nanofibers

Jugroop Singh, Aldwin Pagulayan, Brian A. Camley, Amrinder S. Nain

CONTENTS

I. SUPPLEMENTARY MOVIE LEGENDS

- Movie 1: Protrusions on suspended small (135 nm diameter) fibers. Cells form long protrusions on suspended small diameter fibers. Long protrusions often break from cell body resulting in fragments (white arrows) attached to fibers. Time shown in hours:minutes:seconds:thousandths
- Movie 2: Protrusions formed on suspended large (1000 nm diameter) fibers. Protrusions formed from cells attached to suspended large diameter fibers can be difficult to discern optically. Time shown in hours:minutes:seconds:thousandths
- Movie 3,4: Walk past of spindle shaped cells on suspended fibers (500 nm diameter). Two spindle shaped cells attached to suspended fibers approach each other, make contact and walk past. Time shown in hours:minutes:seconds:thousandths
- Movie 5: Non-mutual CIL in spindle cell pairs on suspended fibers (500 nm diameter). Two spindle shaped cells attached to suspended fibers approach each other and following contact the cell on left (black arrow) repolarizes. Subsequently both cells move together resulting in non-mutual CIL. Time shown in hours:minutes:seconds:thousandths
- Movie 6: Mutual CIL in spindle cell pairs on suspended fibers (500 nm diameter). Spindle shaped cells attached on suspended fibers approach each other and following contact both cells repolarize resulting in mutual CIL. Time shown in hours:minutes:seconds:thousandths
- Movie 7,8: Walk past of spindle shaped cell and daughter cell post division on suspended fibers (500 nm diameter). A spindle shaped cell and a fast-moving daughter spindle shaped cell on suspended fibers approach each other, make contact and walk past. Time shown in hours:minutes
- Movie 9. Non-mutual CIL of spindle shaped cell and daughter cell post division on suspended fibers (500 nm diameter). A slow-moving spindle shaped cell (white arrow) and a fast-moving daughter spindle shaped cell (black arrow) on suspended fibers approach each other, and following contact, the non-dividing cell on right repolarizes. Subsequently both cells move together resulting in non-mutual CIL. Time shown in hours:minutes:seconds:thousandths

- Movie 10. Non-mutual CIL of spindle cell and daughter cell post division on suspended fibers (500 nm diameter). A slow-moving spindle cell (white arrow) and a fast-moving daughter spindle cell (black arrow) approach each other, and following contact, the daughter cell on left repolarizes. Subsequently both cells move together resulting in non-mutual CIL. Time shown in hours:minutes:seconds:thousandths

- Movie 11,12. Non-mutual CIL of parallel-parallel cell pairs on suspended fibers (500 nm diameter). Two parallel cells on suspended fibers approach each other followed by one of the cells (black arrow) repolarizing. Subsequently both cells move together as a train for at least one cell length resulting in non-mutual CIL. Time shown in movie 11 in hours:minutes:seconds:thousandths and in 12: hours:minutes

- Movie 13. Non-mutual CIL of parallel-parallel cell pairs on suspended fibers (500 nm diameter). Two parallel cuboidal shaped cells on suspended fibers approach each other followed by one of the cells (black arrow) repolarizing. Subsequently both cells move together as a train for at least one cell length followed by one of the cells (black arrow) separating. Time shown in hours:minutes:seconds:thousandths

- Movie 14. Non-mutual CIL of parallel-parallel cell pairs on suspended fibers (500 nm diameter). Two parallel cuboidal shaped cells attached on suspended fibers approach each other followed by one of the cells (black arrow) repolarizing. Subsequently both cells move together as a train for at least one cell length followed by one of the cells (white arrow) repolarizing. This results in both cells moving apart from each other. Time shown in movie in minutes

- Movie 15. Walk past of parallel cell in parallel-parallel cell pairs with one cell undergoing division on suspended fibers (500 nm diameter). One parallel cuboidal shaped cell on suspended fibers divides and the daughter cell approaches another parallel cuboidal shaped cell. The daughter cell changes shape to become a spindle shaped cell to achieve walk past. Time shown in hours:minutes:seconds:thousandths

- Movie 16: Walk past of parallel cell in parallel-parallel cell pairs undergoing division on suspended fibers (500 nm diameter). Two parallel cuboidal shaped cells attached on suspended fibers divide and their respective daughter cells approach each other followed by both daughters changing to spindle shape to achieve walk past. Time shown in hours:minutes:seconds:thousandths

- Movie 17. Non-mutual CIL of parallel cell in parallel-parallel cell pairs undergoing division on suspended fibers (500 nm diameter). Two parallel cuboidal shaped cells attached on suspended fibers divide and their respective daughter cells approach each other followed by one of the daughters (black arrow) repolarizing resulting in non-mutual CIL with training. Time shown in hours:minutes:seconds:thousandths

- Movie 18, 19: Push of a parallel by a daughter parallel cell on suspended fibers (500 nm diameter). A dividing daughter cell (white arrow) of a parallel cuboidal cell moving at high speed physically pushes another parallel cuboidal shaped cell (black arrow). Push can be seen by movement of the pushed cell body before formation of visible protrusions. Time shown in hours:minutes:seconds:thousandths

- Movie 20: Leading-trailing edge interactions between spindle cells on suspended fibers (500 nm diameter). A faster moving spindle shaped cell (black arrow) catches up and contacts the trailing edge of slower moving spindle (white arrow) shaped cell resulting in an increase in speed of slower cell. Time shown in hours:minutes:seconds:thousandths

- Movie 21: Leading-trailing edge interactions between spindle cells on suspended fibers (500 nm diameter). A faster moving daughter spindle shaped cell (black arrow) catches up and contacts the trailing edge of slower moving spindle (white arrow) shaped cell resulting in an increase in speed of slower cell. Time shown in hours:minutes:seconds:thousandths

- Movie 22: Leading-trailing edge interactions between parallel cells on suspended fibers (500 nm diameter). A faster moving parallel cuboidal shaped cell (black arrow) catches up and contacts the trailing edge of slower moving parallel (white arrow) cuboidal shaped cell resulting in an increase in speed of slower cell. Time shown in hours:minutes:seconds:thousandths

- Movie 23: Leading-trailing edge interactions between parallel cells on suspended fibers (500 nm diameter). A faster moving daughter parallel cuboidal shaped cell (black arrow) catches up and contacts the trailing edge of slower moving parallel (white arrow) cuboidal shaped cell resulting in an increase in speed of slower cell. Time shown in hours:minutes:seconds:thousandths

- Movie 24. Simulation of spindle-spindle collision showing walk-past. Cell polarity vectors are shown as black lines, and the red, blue cell trajectories over time are traced with the matching color. The fiber is shown as a gray line.

- Movie 25. Simulation of spindle-daughter spindle collision showing walk-past. Cell polarity vectors are shown as black lines, and the red, blue cell trajectories over time are traced with the matching color. The fiber is shown as a gray line.

- Movie 26. Simulation of parallel-parallel collision showing training. Cell polarity vectors are shown as black lines, and the red, blue cell trajectories over time are traced with the matching color. The fiber is shown as a gray line.
- Movie 27. Simulation of parallel-parallel daughter collision showing walk-past. Cell polarity vectors are shown as black lines, and the red, blue cell trajectories over time are traced with the matching color. The fiber is shown as a gray line.
- Movie 28. External probe pushing on a spindle cell on a suspended fiber (500 nm diameter). A computer-controlled glass probe pushes on a spindle shaped cell causing it to move about the suspended fiber
- Movie 29: Daughter cells after mitosis apply contractile forces causing 500 nm diameter fibers to deflect inwards. Time shown in hours:minutes:seconds:thousandths
- Movie 30: Walk past of non-dividing parallel-parallel cell pairs in calcium-free medium on suspended fibers (500 nm diameter). Two parallel cuboidal shaped cells in calcium-free media attached on suspended fibers approach each other, make contact, and walk past. Time shown in hours:minutes:seconds:thousandths
- Movie 31: Tracing of spindle cells during collision in a walk past interaction. As two spindle cells make contact and walk past, cell tracing was used to track cells and perform measurements. Time shown in hours:minutes.

II. SUPPLEMENTARY FIGURES

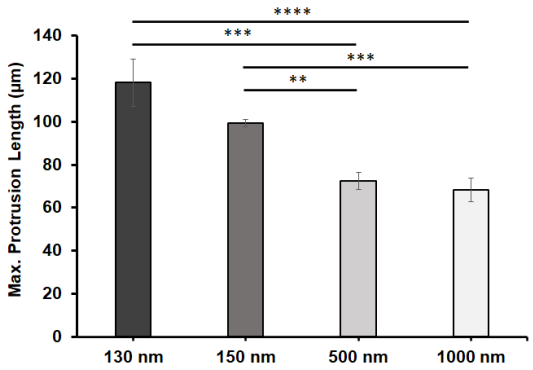

FIG. S1. Maximum protrusion length of cells on fibers of diameter 130 nm, 150 nm, 500nm, and 1000nm. (****, $p < 0.0001$; ***, $p < 0.001$; **, $p < 0.01$; *, $p < 0.05$).

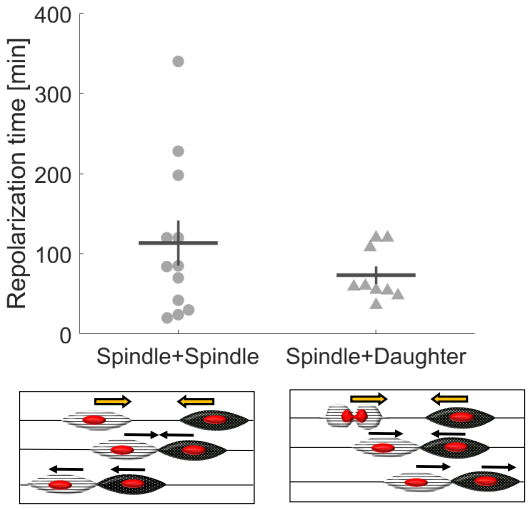

FIG. S2. Time to repolarize for spindle-spindle and spindle-daughter collisions that lead to train formation. $n = 12, 9$ respectively. $p = 0.25$.

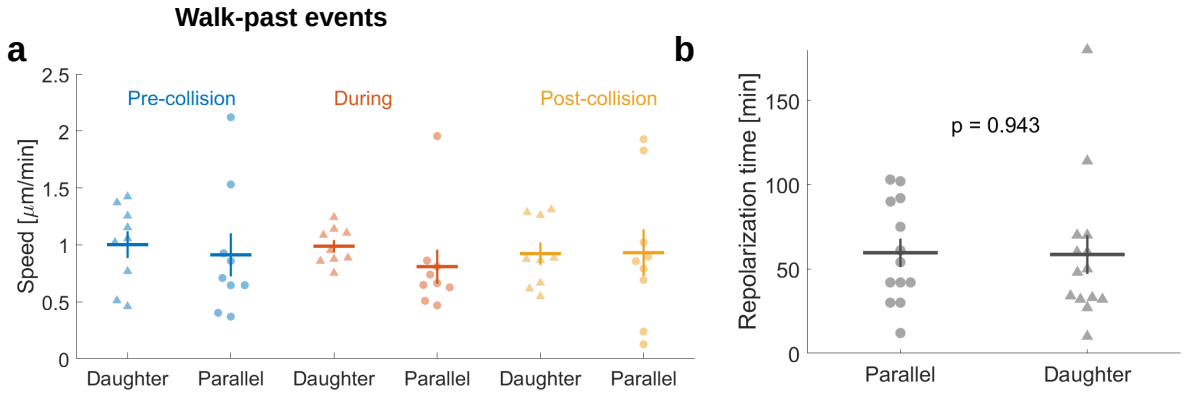

FIG. S3. Speeds and repolarization times for parallel collisions. **a)** Speed during walk-past events, which necessarily require one cell to be a daughter. None of the differences tested here have $p < 0.05$. **b)** Comparison between repolarization time for parallel-parallel and parallel-daughter events. The repolarization times for parallel-daughter events include both events we considered "push" and those we did not.

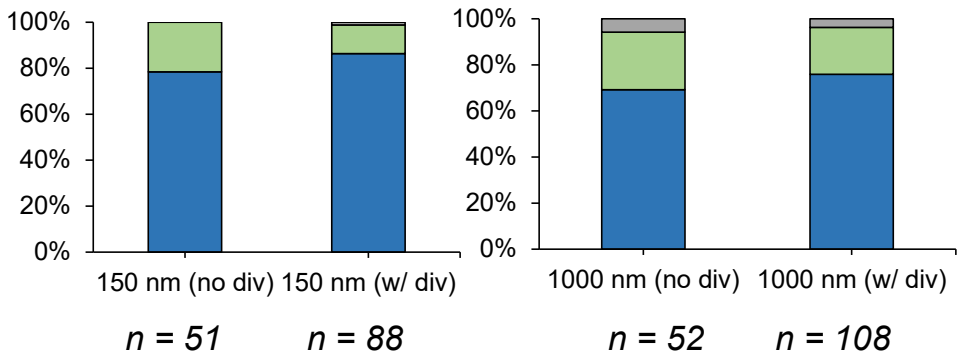

FIG. S4. Outcomes for spindle cells on 150 nm and 1000 nm fibers. Blue (bottom bar) indicates walk-past, green (middle bar) is non-mutual CIL (training), and gray (top bar) is mutual CIL (reversal).

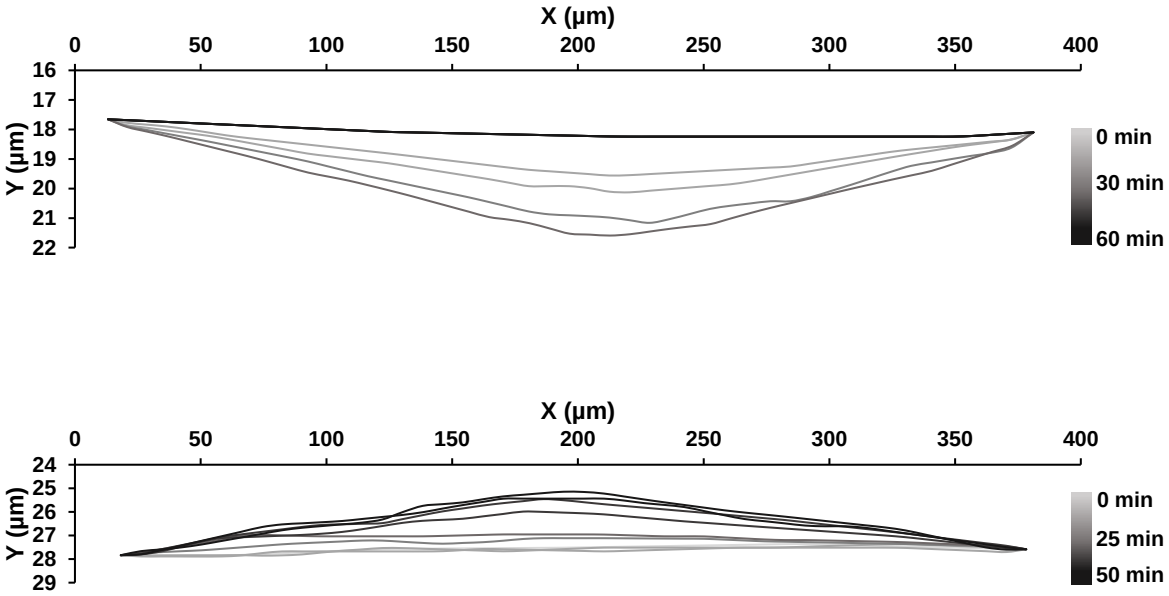

FIG. S5. Additional examples of fiber deflections during division.

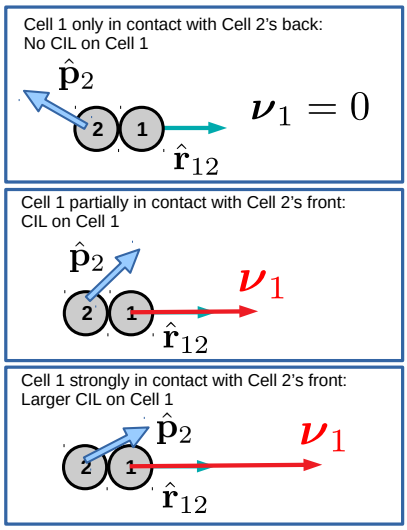

FIG. S6. Relative strengths of CIL in model depending on orientation of cells. We note that generally, cells are oriented along the $\pm x$ direction, so the orientations shown are not particularly realistic.

III. MODEL DETAILS

We extend the model of [1] to describe interacting cells attached to a fiber. We model cells $i = 1, 2$ as having a polarity $\mathbf{p}_i$. Polarity is the velocity a cell *would* travel with if there were no mechanical forces acting on the cell (e.g. from other cells, the fiber) – its units are of velocity. This polarity obeys an equation:

$$\frac{d}{dt}\mathbf{p}_i = \underbrace{-\frac{1}{\tau}\mathbf{p}_i}_{\text{Relaxation}} + \underbrace{\frac{1}{\tau}\hat{\mathbf{x}}v_{cg}\frac{\mathbf{p}_i\cdot\hat{\mathbf{x}}}{|\mathbf{p}_i\cdot\hat{\mathbf{x}}|}}_{\text{contact guidance}} + \underbrace{\beta\boldsymbol{\nu}_i}_{\text{CIL}} + \underbrace{\sigma\boldsymbol{\xi}_i(t)}_{\text{Gaussian noise}} \tag{S1}$$

There are four terms:

- **Relaxation.** In the absence of any other terms, polarization relaxes to zero with the time τ. This provides a characterization of the cell's persistence time in one direction.
- **Contact guidance.** Promotes polarization along the fiber axis (which we choose as $\hat{\mathbf{x}}$). If $p_x > 0$, this term polarizes the cell along $+\hat{\mathbf{x}}$, otherwise along $-\hat{\mathbf{x}}$. The term τ^{-1} in front means that, with only the first two terms, the cell will tend to relax to $p_x = \pm v_{cg}$ over a timescale τ.
- **CIL.** This term biases cells away from contact with their neighbors, into the direction $\boldsymbol{\nu}_i$:

$$\boldsymbol{\nu}_i = \sum_{j\sim i}\hat{r}_{ij}\left(\hat{r}_{ij}\cdot\hat{\mathbf{p}}_j\right)\Theta\left(\hat{\mathbf{r}}_{ij}\cdot\hat{\mathbf{p}}_j\right) \tag{S2}$$

  where the sum is over cells j neighboring i ($j \sim i$), i.e. those within a distance $2R$ from the cell, $\hat{r}_{ij} = (\mathbf{r}_i - \mathbf{r}_j)/|\mathbf{r}_i - \mathbf{r}_j|$ is the unit vector connecting cells i and j and $\hat{\mathbf{p}}_i = \mathbf{p}_i/|\mathbf{p}_i|$. $\Theta(x)$ is the Heaviside step function, $\Theta(x) = 0$ for $x < 0$, $\Theta(x) = 1$ for $x > 0$. The intuition for this term is shown in Figure S6 – the direction $\hat{\mathbf{r}}_{ij}$ points away from the neighbor j, modeling CIL – but CIL only happens when a cell is in contact with the front of another cell. The term $\hat{\mathbf{r}}_{ij}\cdot\hat{\mathbf{p}}_j$ ensures that this CIL will be stronger if the front is more aligned with the cell-cell contact axis – representing that CIL will be stronger if more of the front of one cell is in contact with one another. **This term differs from that in [1] because we assume only contact with another cell's front leads to repolarization.** This was found to be important in more complex models like [2, 3] and is one way for a CIL-like mechanism to create streams of cells. This asymmetry between front and rear contact has been experimentally observed [4, 5], and is consistent with our experimental observation of train formation. However, we note that symmetric interactions can also lead to train formation [6].
- **Gaussian noise**. This last term is a white Gaussian Langevin noise; this fluctuation would drive the cell to have a persistent random walk in the absence of other features. With just relaxation and noise, the resulting "Ornstein-Uhlenbeck" model [7, 8] would have a Gaussian distribution of $\mathbf{p}$. For simplicity, we have chosen this noise to be isotropic, so that the

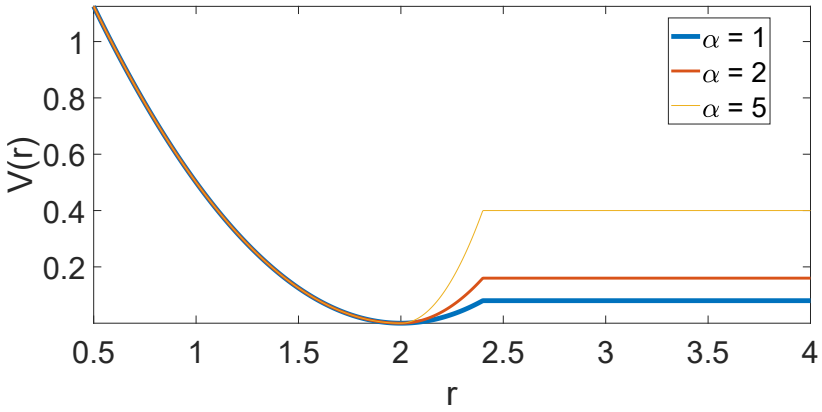

FIG. S7. Cell-cell interaction potential includes short-range repulsion and short-range attraction. Beyond the distance R_{adh}, the potential is constant (zero force). This is only illustrative and does not match the parameters in the paper – this graph shows $R = 1$ and $R_{\text{adh}} = 1.2$.

amplitude of changes in polarization along the cell's polarization, which cause changes in speed, are the same as those perpendicular to the cell's polarization, which would cause the cell to tend to rotate around the fiber. This is consistent with our observations that cells do spontaneously rotate around the fiber axis. Extending the model to allow these values to be different could change the specific quantitative dependence on the parameter σ shown in Fig. S9.

How does the polarity $\mathbf{p}_i$ of each cell translate into its motion? The motion of cells is at low Reynolds number (highly overdamped). We then write the cell's velocity as

$$\frac{d}{dt}\mathbf{r}_i = \mathbf{p}_i - \mu\frac{\partial U_{\text{fiber}}(\mathbf{r}_i)}{\partial \mathbf{r}_i} - \mu\frac{\partial U_{\text{cell-cell}}(\{\mathbf{r}\})}{\partial \mathbf{r}_i} \tag{S3}$$

where μ is a mobility coefficient for the cell, i.e. a constant force F_z on a cell leads to a constant velocity $v_z = \mu F_z$. The term U_{fiber} keeps the cell pinned to the fiber(s):

$$U_{\text{fiber}}(\mathbf{r}) = \frac{\kappa}{2}\left[(\rho_1 - R)^2 + (\rho_2 - R)^2\right] \tag{S4}$$

where $\rho_1 = \sqrt{y^2 + z^2}$ is the distance from the first fiber (the x axis) and $\rho_2 = \sqrt{(y-\Delta)^2 + z^2}$ is the distance from a second fiber. (If only one fiber is simulated, as in spindle simulations, only the first term is included.) The typical distance of separation between the fiber and the cell center of mass is taken to be R, the radius of the cell. This is appropriate if the fiber is, as in our case, much smaller than the cell radius. This energy reflects the fact that if a cell is pulled away from the fiber ($\rho > R$), it must deform – but so must cells compressed close to the fiber ($\rho < R$).

Cell-cell interactions are are composed of a short-range repulsion, representing the elastic deformation of the cells as they become closer to one another, and a longer-range adhesion, which states that for cells in contact to be pulled apart, force must be applied to them. These potentials are:

$$U_{\text{cell-cell}} = \frac{1}{2}\sum_{i\neq j} V(|\mathbf{r}_i - \mathbf{r}_j|) \tag{S5}$$

with an interaction energy

$$V(r) = \begin{cases} \frac{1}{2}\kappa_{\text{cell}}(r-2R)^2 & r < 2R \\ \frac{1}{2}\alpha(r-2R)^2 & r \in [2R, 2R_{\text{adh}}] \\ \frac{1}{2}\alpha(2R_{\text{adh}}-2R)^2 & r > 2R_{\text{adh}} \end{cases} \tag{S6}$$

where κ_{cell} is the spring constant of the cell-cell interaction, α characterizes the strength of adhesion, and R_{adh} is the radius of adhesion (two cells separated by more than $2R_{\text{adh}}$ feel no adhesive force). Note that overlap begins at separations $r < 2R$, as R is the cell radius, not its diameter. This potential is shown for different values of α in Fig. S7 – larger values of α correspond to a larger adhesion (i.e. a larger force required to rupture one cell from another).

IV. SIMULATION PROTOCOL

We simulate cell-cell collisions on a fiber. To set up each collision, we first simulate the cells without any physical cell-cell interactions or CIL for a time T_{relax} (setting $\beta = 0, \alpha = 0, \kappa_{\text{cell}} = 0$); this ensures that the cells have polarities $\mathbf{p}_i$ that are

sampled according to the steady-state distribution of individual cells – i.e. that this represents a random cell. We then set up the cells to collide, choosing their x separation to be $x_{\text{init}} = 3R$. (We keep their y and z values to be the values generated by the initial evolution without cell-cell interactions). We also choose the cell polarities to be pointing toward one another, so that head-head collisions are the likely outcome. (We do this by ensuring that the cell that has the larger x has a negative p_x and the cell with a smaller x has positive p_x. If necessary, we flip the sign of one of the cell's p_x values; this is permitted because in the absence of interactions $p_x \to -p_x$ is a symmetry of our polarity equation.) After this setup, we run the simulation for a time T_{sim} and track the outcome.

In modeling collisions where one cell has recently divided, we first perform the relaxation as above, but for the cell which has divided, we multiply its polarity along the axis p_x by a factor M. We note that the initial polarity p_x for each cell is set by the relaxation process, and so is random; this means that the daughter cell's p_x is not necessarily larger than the other cell's p_x, reflecting the large variability in speeds.

We run $N_{\text{it}} = 200$ head-head collisions for each set of parameters and automatically classify the outcomes with the rules:

- **No contact.** If the cells never reach an r separation of $2R_{\text{adh}}$ (i.e. they never interact), we note this as a non-collision; outcome fractions are computed as fractions of collision events.
- **Reversal.** A collision is marked as a reversal if the cells contact, then separate by x_{init} with the cell at initially lower x remaining at lower x
- **Walk-by.** A collision is marked as walk-by if the cells contact, and the x positions of the cells exchange (the cell at smaller x is above the cell at higher x). If a trajectory could be counted as either walk-by or reversal (due to multiple collisions), whichever event occurs first is counted.
- **Train/stalling/push.** If the cells have contacted but not separated more than x_{init}, we count the collision as a training event or stalling. (This would also encompass a pushing event.) Because cells in contact will eventually polarize and move as a train, we do not distinguish between these different outcomes in our statistics.

V. EFFECT OF CHANGING PARAMETERS ON OUTCOMES

In this section, we take our best fit parameters (Table S3) as our "wild type" and show how the outcomes depend on varying key parameters. We show this for four cases: head-head collisions in the spindle geometry, in the parallel geometry, spindle with a division, and parallel with a division. In all cases, up-regulating the adhesion strongly suppresses walk-past and promotes train formation (Fig. S8a): if cells are not able to separate from one another, they will move together. Another relevant parameter is the degree of attachment between the cell and the fiber(s) – essentially the strength of the spring holding the cell to the surface of the fiber. We find that this primarily plays a role when the cells are attached to two fibers: in the parallel geometry, increasing this strength suppresses walk-by (Fig. S8b), though it has little effect in the single-fiber geometry. This is again intuitively likely: for cells to walk past each other in the parallel geometry, they must move away from their preferred position precisely between the two fibers – and this is suppressed by increasing the adhesion to the fiber. Perhaps surprisingly, the strength of CIL β only weakly regulates outcomes, tending to promote training and suppress walk-past (Fig. S8c). This relatively weak dependence on β is in part because we have not distinguished in our outcomes between cells that turn around rapidly on contact, and those that take larger times to repolarize.

Walk-past can be strongly increased by having cells with larger polarity noise σ – cells with more variable velocities are likelier to walk past each other (Fig. S9a). However, we find no apparent effect from changing the cell's stiffness itself (Fig. S9b), likely reflecting that the cell stiffness found in the fit is relatively high. In addition, we see that our time step does not significantly influence rates (Fig. S9c), showing that the simulations are numerically converged.

The degree to which a cell is repolarized on division does regulate the outcomes of cell-cell collisions with dividing cells. Increasing M increases the rate of walk-past when division occurs, as would be expected (Fig.S10a). Persistence time τ also regulates walk-past, with larger τ values corresponding to more walk-past (Fig.S10b). This effect also reflects that the persistence time term opposes fluctuations – cells with a larger persistence time will have larger-amplitude velocity fluctuations for a fixed σ, so this is consistent with our results for changing σ. Increasing the contact guidance velocity v_{cg} increases walk-past as well (Fig.S10c).

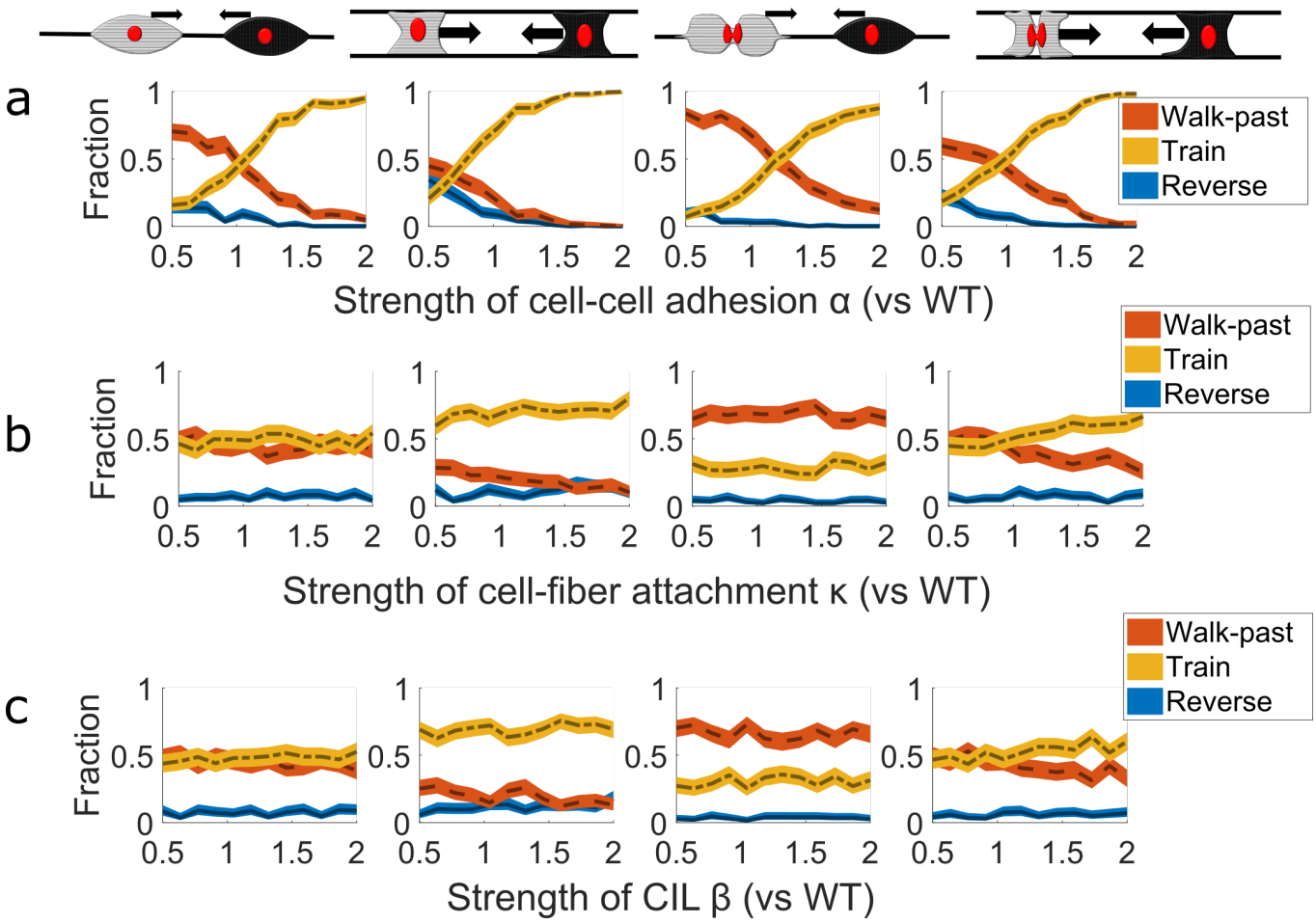

FIG. S8. **Biophysical parameters controlling the relative rates of different outcomes.** The fraction of each outcome is shown as a function of a single parameter being varied relative to its "WT" (best fit to experimental data) value. Shown are a) cell-cell adhesion strength, b) cell-fiber attachment strength, and c) strength of CIL. The four columns show the four collision types – spindle-spindle, parallel-parallel, spindle-daughter, and parallel-daughter. Shaded regions indicate 95% confidence interval, computed via the Goodman method [9] assuming the distribution of outcomes is multinomial. Each point on the lines is computed from 200 individual simulations.

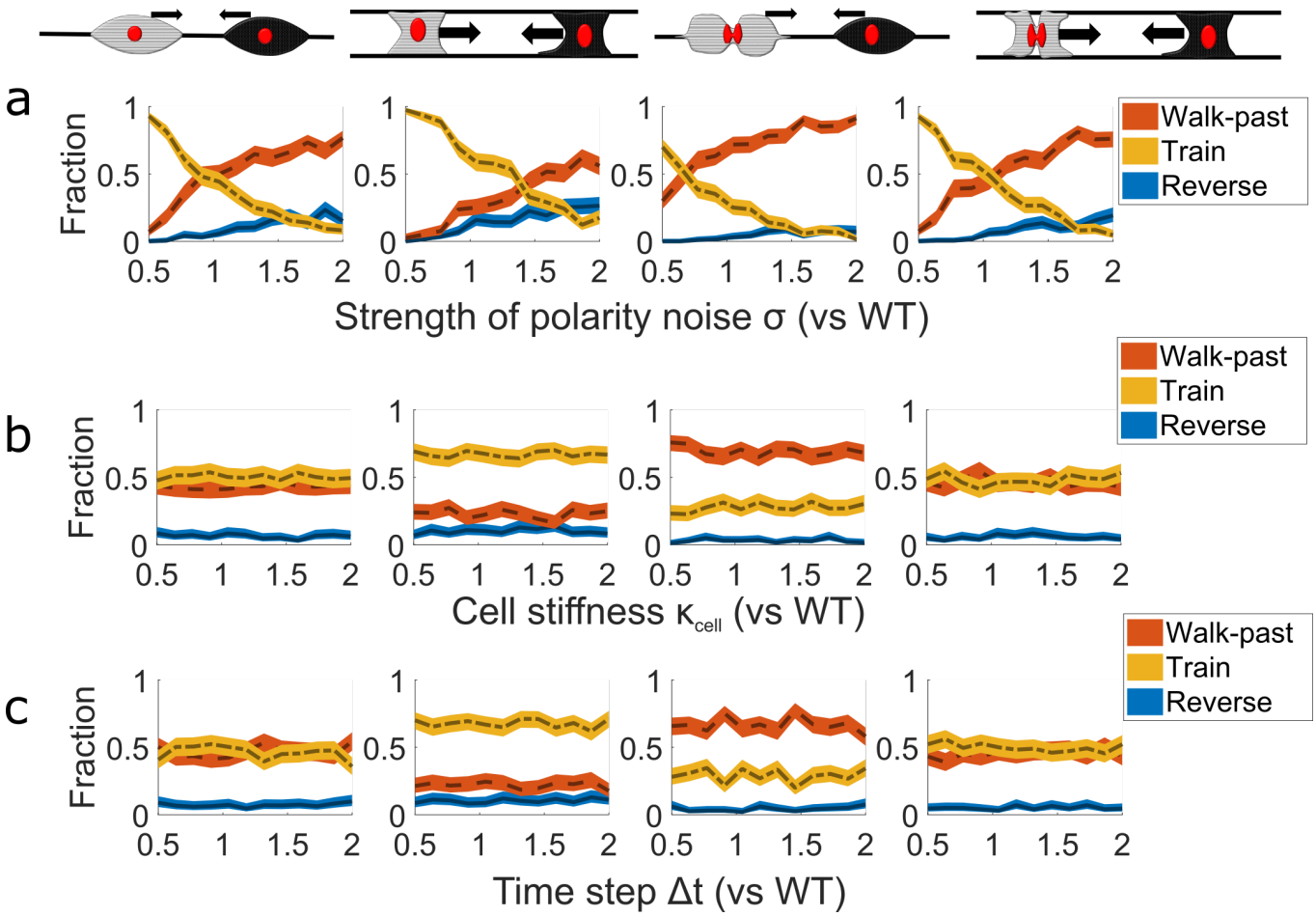

FIG. S9. **More biophysical and computational parameters controlling the relative rates of different outcomes.** The fraction of each outcome is shown as a function of a single parameter being varied relative to its "WT" (best fit to experimental data) value. Shown are a) cell polarity noise σ, b) cell stiffness κ_{cell}, and c) the time step Δt. The four columns show the four collision types – spindle-spindle, parallel-parallel, spindle-daughter, and parallel-daughter. Shaded regions indicate 95% confidence interval, computed via the Goodman method [9]. Each point on the lines is computed from 200 individual simulations.

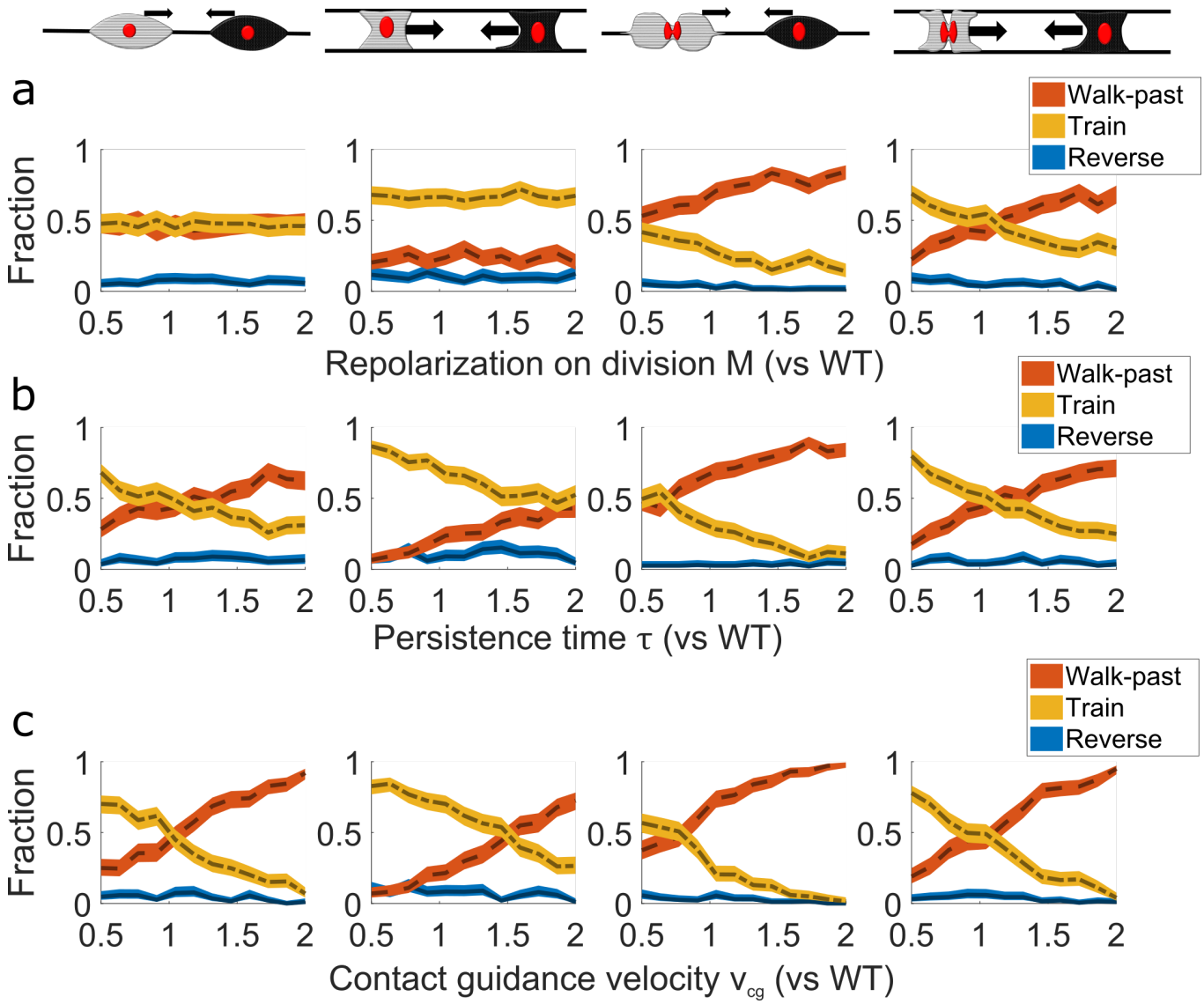

FIG. S10. **Yet more biophysical and computational parameters controlling the relative rates of different outcomes.** The fraction of each outcome is shown as a function of a single parameter being varied relative to its "WT" (best fit to experimental data) value. Shown are a) change in polarity of dividing cells M, b) cell persistence time τ, and c) the contact guidance velocity v_{cg}. The four columns show the four collision types – spindle-spindle, parallel-parallel, spindle-daughter, and parallel-daughter. Shaded regions indicate 95% confidence interval, computed via the Goodman method [9]. Each point on the lines is computed from 200 individual simulations.

VI. PARAMETER FITTING AND VARIATION

A. Fixed parameters

We show parameters that are fixed through all our fitting process in Tables S1 and S2. We note that these parameters (except the fiber spacing) are also kept constant between spindle and parallel simulations; we have taken a minimal approach and not directly treated changes in, e.g. persistence time or v_{cg} between spindle and parallel. All of the effects of the spindle-parallel geometry change in the simulation is due to the presence of the additional fiber.

TABLE S1. Table of fixed biological model parameters

Parameter	Name	Value	Units	Justification
τ	Persistence time	3	hours	Measured from our experiments showing that cells lose their post-division additional velocity in ~ 3 hours.
v_{cg}	Contact guidance velocity	18	μm/hr	Estimated from typical time-averaged x cell velocities in our experiment
M	Effect of division	3	unitless	Rough estimate from experiments; this reflects the increase in a time-averaged speed along the x axis, not merely the instantaneous speed in any direction.
R	Cell radius	25	μm	Rough order of magnitude from experiment. We note that "radius" of a cell here will always be a little misleading because the cells are extremely elongated; we chose this value to be a compromise between the typical cell extent in the long and short axes
R_{adh}	Adhesion radius	30	μm	Must be larger than cell radius
Δ	Fiber spacing	50	μm	Chosen to be exactly $2R$ so that one cell fits precisely between fibers

TABLE S2. Table of parameters related to simulation details

Parameter	Name	Value	Units	Justification
Δt	Time step	0.01	hr	Set by convergence
x_{init}	Initial separation	3 R	μm	Set to be relatively small so a high fraction of cells collide.
T_{relax}	Equilibration time	30	hr	This is the time for which we simulate each cell in isolation before we set them up to collide. This is set to be much longer than the cell persistence time.
T_{sim}	Simulation time	15	hr	Time which is simulated for each collision; if cells have not contacted during this time, no collision is counted.

B. Parameters that are varied

The parameters shown in Table S3 are used in two different ways. First, we generate a plausible range of parameters, and evaluate collision statistics over a sample enclosing that whole range, generating a large number of different plausible parameter sets. We show in the main paper that the main qualitative conclusions are robust to these parameter variations (Figure 5 of the main paper). Secondly, we find a best global fit to the observed experimental outcomes (e.g. spindle-spindle collisions producing 66% walk-past; the comparison is Figure 6 of the main paper). Both the range and the best fit are shown in Table S3.

To generate the range of representative parameters, we used Latin hypercube sampling, so that many combinations of parameters were explored. Because the plausible range of the parameters β, κ, and κ_{cell} were large, we chose our sampling to be logarithmically spaced over the plausible range.

To find our best fit, we minimized the mean-square error of the fractions f_i of events between experiment and simulation (using $N_{\text{it}} = 200$ iterations). The minimization was done with Nelder-Mead unconstrained optimization (MATLAB's fminsearch), starting from the minimal error point found in the Latin hypercube sample. We have also put in a small penalty term to changing σ, which is more closely constrained by the data.

TABLE S3. Table of parameters related to simulation details

Parameter	Name	Plausible range	Best fit	Units	Justification
σ	Noise strength	8.57-15.91	12.21	$\mu m\,\mathrm{hr}^{-3/2}$	Range chosen so that typical velocity standard deviation $\sqrt{\sigma^2\tau/2}$ is roughly 0.25 microns/min, to be consistent with observed variance in velocities; we have included a range of possible variation of 30% around this value, as we suspect it is not well-constrained due to small sample size
$\kappa\mu$	Strength of fiber-cell attachment	1-50	1.81	hr^{-1}	κ has units of a spring constant, but it only enters into our model in the combination $\kappa\mu$. This range encompasses both values where the cell is tightly attached to the filament and cannot be pulled from it and those where it is more easily stretched from contact with the filament, but rules out parameters where a single cell will spontaneously move away from contact with the wires. *Note: To interpret this and other adhesion strengths/stiffnesses with these units, it's useful to think that* $\kappa\mu = 10/hr$ *means that under a deformation of* 1 *micron, the responding velocity of the cell is* $\kappa\mu \times 1micron = 10micron/hr$.
$\kappa_{\text{cell}}\mu$	Cell stiffness	10-50	23.7	hr^{-1}	κ_{cell} is a spring constant, but it only enters into our model in the combination $\kappa_{\text{cell}}\mu$. This range of values is set so that the cell-cell repulsion is strong enough that cell overlaps are not common – this requires $\kappa_{\text{cell}}\mu \sim O(10)\mathrm{hr}^{-1}$
$\alpha\mu$	Strength of cell-cell adhesion	2.2-4	3.11	hr^{-1}	α is a spring constant, entering into the model only as $\alpha\mu$. This range is chosen because if $\alpha\mu$ is much outside this range, either cell-cell adhesion will be too weak to strongly affect cell-cell interactions or so strong that cells in contact will never be able to separate. Our conclusions also hold if we allow $\alpha\mu$ to be much smaller (Fig.S12).
β	CIL strength	8-40	15.4	hr^{-1}	We know that, in order to create a relevant effect, we must have $\beta\tau$ – the maximum velocity that can be induced by CIL – on the order of cell velocities (20 microns/hr). We chose the low end of this range to ensure that cells in contact did repolarize – at the high end, the induced velocities become unreasonable.

C. Interpretation of best fit parameters

Our fitting process identified parameters $\kappa\mu$, $\kappa_{cell}\mu$, $\alpha\mu$, β, and σ. We see that the best-fit parameters have a cell stiffness that is much larger than the cell-fiber attachment stiffness, which might be surprising. Interpreting these two mechanical parameters from our minimal model, however, is not simple, because of how we summarize the complex shape of the cell as a single point. Motion of the cell away from the fiber, which is penalized by κ, involves both changing the cell shape and deforming the cell-fiber attachment. Based on our experimental videos, we expect that changes in cell shape are the largest component of this stiffness. Essentially, $\kappa_{cell} \gg \kappa$ is a statement that cells more easily displace their center of mass from the ideal location of the fiber than they do in cell-cell collisions. Without this condition, cells would be able to unphysically crawl through one another.

The parameter κ controls the strength of the effective attachment between the cell centroid and the fiber. Can we check that our value is physically reasonable? One way to do this would be to look explicitly at the fluctuations away from the fiber axis ($y = 0$ in the experiment) for non-colliding cells. We show this data in Fig.S11, computing the change Δy of the cell's centroid away from its equilibrium position over the period of the measurement. However, direct comparison between the experiment and simulation is made difficult because of the shape and size differences between cells, making this comparison qualitative

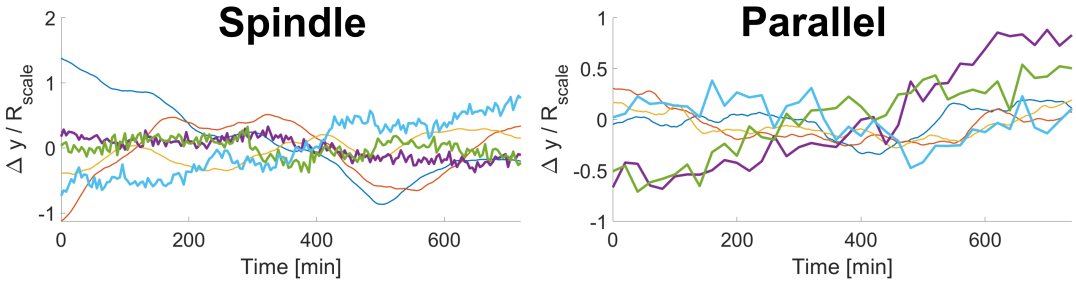

FIG. S11. Comparison between experimental (heavy, noisier lines) and theoretical (lighter lines) fluctuations away from their typical positions shows that cells can move from one side of the fiber to the other over similar time scales, though this comparison is made difficult and confounded by the shape dynamics in the experiment (see text).

rather than quantitative. In approximating our cells by spheres, we chose $R = 25\mu m$, as a compromise between their large length and much smaller size perpendicular to the fiber. For this reason, the values of Δy for the simulation are on the order of 25 microns – unavoidable given the cell's size – while the values for the experiment are on the order of < 5 microns. We have thus presented these values Δy scaled by $R_{scale} = 25\mu m$ for the simulations and $5\mu m$ for the experiments. We also note that to avoid overcomplicating the model, we did not change the cell size between spindle and parallel – but the cell size perpendicular to the fiber is larger in parallel experiments than in spindle experiments. At a qualitative level, we find in Fig.S11 that both in simulation and experiment, we see that in both simulation and experiment, $\Delta y/R_{scale}$ can change significantly – on the order of 1 – over similar timescales of about 600 minutes. This provides a rough sense that the fluctuations of the cell around the fiber are reasonable, but unfortunately cannot be used for quantitative parameterization due to the problems in mapping between the complex shape of the cell and the spherical shape assumed in the model.

VII. MODEL ROBUSTNESS TO EXTENDED PARAMETER VARIATIONS

Throughout the paper and supplement, we have kept the parameters v_{cg} and M fixed unless otherwise stated. We show now that the central conclusions shown in Fig. 5c of the main paper do not depend on this assumption. In Fig S12, we show 200 parameters selected using Latin hypercube sampling, as in the main paper, using parameters sampled from the fit range shown in Table S3. In addition, however, we have extended the range of adhesion, allowing $\alpha\mu$ to range from 0.1 to 4 hr^{-1}, and allowed M to vary from 2 to 4 and v_{cg} to vary from 12 to 24 μm/hr. We find that, as in the main paper, spindle cells always walk-past at greater rates than parallel cells, and division never decreases walk-past rates. As in the main paper, we see examples where walk-past is not increased by division, e.g. when cells are so strongly adherent to two fibers that they cannot walk past each other.

[1] B. A. Camley, J. Zimmermann, H. Levine, and W.-J. Rappel, Emergent collective chemotaxis without single-cell gradient sensing, Physical Review Letters **116**, 098101 (2016).

[2] B. A. Camley, Y. Zhang, Y. Zhao, B. Li, E. Ben-Jacob, H. Levine, and W.-J. Rappel, Polarity mechanisms such as contact inhibition of locomotion regulate persistent rotational motion of mammalian cells on micropatterns, Proceedings of the National Academy of Sciences **111**, 14770 (2014).

[3] D. A. Kulawiak, B. A. Camley, and W.-J. Rappel, Modeling contact inhibition of locomotion of colliding cells migrating on micropatterned substrates, PLoS Computational Biology **12**, e1005239 (2016).

[4] R. A. Desai, S. B. Gopal, S. Chen, and C. S. Chen, Contact inhibition of locomotion probabilities drive solitary versus collective cell migration, Journal of The Royal Society Interface **10**, 20130717 (2013).

[5] D. Li and Y.-l. Wang, Coordination of cell migration mediated by site-dependent cell–cell contact, Proceedings of the National Academy of Sciences **115**, 10678 (2018).

[6] B. A. Camley and W.-J. Rappel, Velocity alignment leads to high persistence in confined cells, Physical Review E **89**, 062705 (2014).

[7] D. Selmeczi, S. Mosler, P. H. Hagedorn, N. B. Larsen, and H. Flyvbjerg, Cell motility as persistent random motion: theories from experiments, Biophysical Journal **89**, 912 (2005).

[8] N. G. Van Kampen, *Stochastic Processes in Physics and Chemistry*, Vol. 1 (Elsevier, 1992).

[9] L. A. Goodman, On simultaneous confidence intervals for multinomial proportions, Technometrics **7**, 247 (1965).

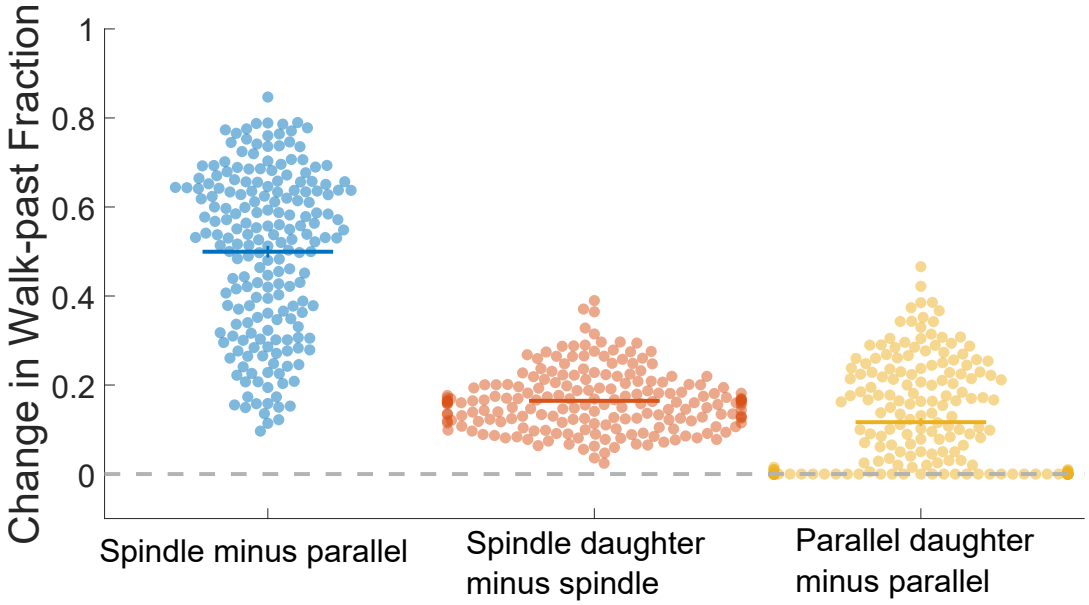

FIG. S12. Central conclusions from main paper are preserved even when more parameters are varied simultaneously.